RSC Advances

PAPER

View Article Online
View Journal | View Issue

Cite this: *RSC Adv.*, 2025, **15**, 5965

Enhancing the photovoltaic properties of phenylsulfonyl carbazole-based materials by incorporating a thiophene ring and end-capped acceptors for organic solar cells: a DFT approach†

Muhammad Khalid, *[ab] Laiba Amir,[ab] Muhammad Arshad,[c] Iqra Shafiq,[ab] Ataualpa Albert Carmo Braga [d] and Khalid Abdullah Alrashidi[e]

Received 22nd August 2024
Accepted 6th February 2025

DOI: 10.1039/d4ra06073c

rsc.li/rsc-advances

In the present study, phenylsulfonyl carbazole-based organic chromophores, abbreviated as **PSCD1–PSCD6**, were designed through tailoring the terminal group of a **PSCR** chromophore. Quantum chemical studies were carried out using the M06/6-311G(d,p) functional to understand the electronic, structural, chemical, and optical properties of the title chromophores. All the derivatives exhibited reduced band gaps with ΔE = 2.742–3.025 eV and significant bathochromic shifts with λ_{max} = 496.891–545.009 nm compared with **PSCR**. DOS and TDM investigations revealed that the central acceptor moiety plays a crucial role in charge transfer. The minimal binding energy values for **PSCD1–PSCD6** indicated a greater rate of exciton dissociation and more effective charge transfer than **PSCR**. The studied compounds exhibited open-circuit voltages (V_{oc}) ranging from 1.015 to 1.720 V. **PSCD4** showed a significantly reduced band gap of 2.742 eV and a red-shifted absorption maximum of 545.009 nm, among all the studied chromophores. These findings suggest that all the designed organic chromophores might be utilized as reasonable photovoltaic materials.

Introduction

Solar energy is an abundant, renewable resource that could enhance environmental health by minimizing the ecological impacts associated with fossil fuels.[1,2] Through efficient harnessing, it can support the drive toward a sustainable energy future and efforts to mitigate pollution and reduce greenhouse gas emissions.[3] Organic solar cells (OSCs) have emerged as a promising technology within this framework owing to their unique qualities, such as flexibility, light weight, and compatibility with roll-to-roll manufacturing.[4] Typically, OSCs consist of a bulk heterojunction (BHJ) structure, where electron donor and acceptor materials are blended to enhance charge separation and energy conversion.[5] By carefully designing and optimizing the morphologies of these donor and acceptor components, scientists have developed OSCs capable of achieving impressive power conversion efficiencies (PCEs) of up to 19.9%.[6] This efficiency stems from the capacity of OSCs to absorb light across a broad spectrum, from the visible to the infrared region, and their molecular flexibility allows tuning of their energy gaps to maximize light absorption.[7] Consequently, OSCs are considered a viable solution for eco-friendly energy generation and could contribute to the transformation of the current energy system to a sustainable, lower-impact energy grid.[8,9]

Among the many classes of OSCs, fused-ring electron acceptors with an A1–π–A2–π–A1 configuration are widely used in OSCs.[10] Various molecular configurations, such as D–π–D–π–A, A–π–D–π–A, A–π–A–π–A, D–π–A, and A–π–A, have been extensively studied to optimize the photovoltaic properties of OSCs. Introducing strong electron-withdrawing groups on terminal acceptor moieties, coupled with a donor unit core, significantly reduces band gaps and binding energies. This approach also broadens the absorption spectrum as well as enhances the exciton dissociation rate and open-circuit voltage of OSCs.[11]

OSCs based on (phenylsulfonyl)-7*H*-benzofuro[2,3-*b*]carbazole derivatives exhibit several advantageous properties for use in solar cells, including strong light absorption, finely tunable energy levels, and excellent charge-transport characteristics. Their potential to improve the efficiency and stability of OSCs

[a]*Institute of Chemistry, Khwaja Fareed University of Engineering & Information Technology, Rahim Yar Khan, 64200, Pakistan. E-mail: muhammad.khalid@kfueit.edu.pk; Khalid@iq.usp.br*

[b]*Centre for Theoretical and Computational Research, Khwaja Fareed University of Engineering & Information Technology, Rahim Yar Khan, 64200, Pakistan*

[c]*Industry Solutions, Northern Alberta Institute of Technology, Edmonton, Alberta, Canada*

[d]*Departamento de Química Fundamental, Instituto de Química, Universidade de São Paulo, Av. Prof. Lineu Prestes, 748, São Paulo, 05508-000, Brazil*

[e]*Department of Chemistry, College of Science, King Saud University, P. O. Box 2455, Riyadh 11451, Saudi Arabia*

† Electronic supplementary information (ESI) available. See DOI: https://doi.org/10.1039/d4ra06073c

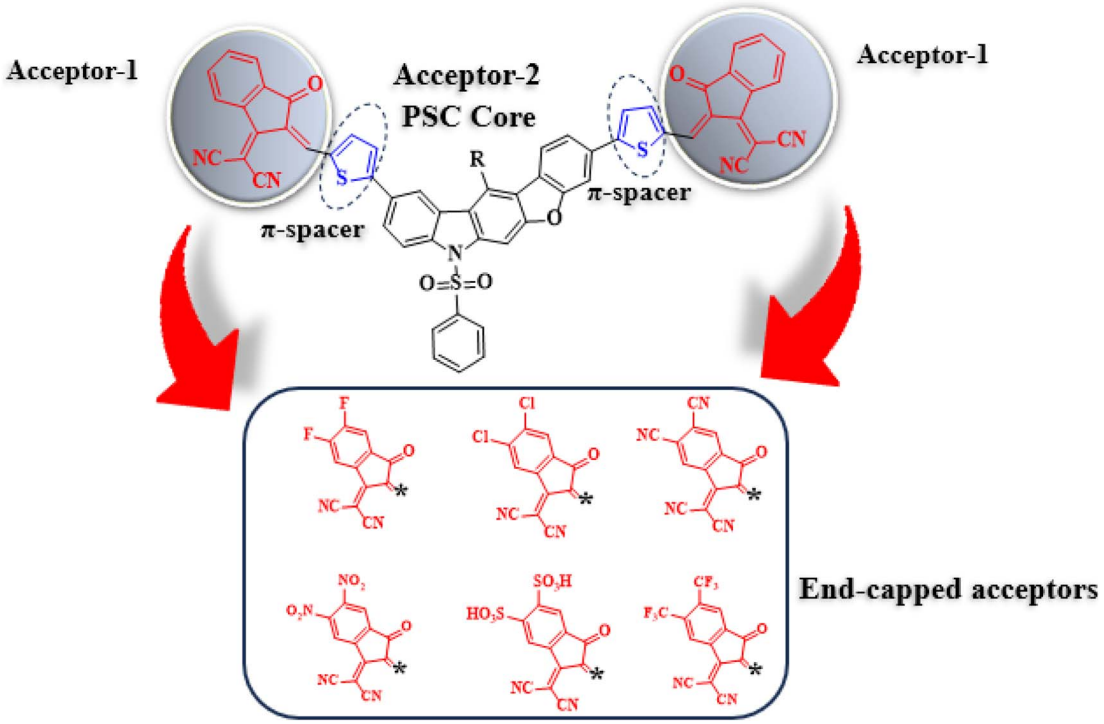

Fig. 1 Modification of the reference compound (PSCR) to design its derivatives using different end-capped acceptor moieties.

makes them valuable candidates for further research and development in the field of photovoltaics.[12] This class of materials combines the electroactive and photophysical benefits of both carbazole and benzofuran structures, resulting in high charge mobility and stability. The carbazole core possesses a rigid planar structure, which promotes effective π–π stacking interactions and efficient charge transport within the photovoltaic material. Additionally, carbazole's relatively high oxidation potential makes it suitable for use in the hole-transport layer, improving charge separation and reducing recombination losses in devices. Because of these features, carbazole is considered a highly significant and versatile building block in the development of high-performance photovoltaic materials, contributing to improving the absorption of light and efficiency of organic solar cells.

Carbazoles have been investigated for fabricating luminescent and hole-transporting materials,[13] organic semiconductors, high-performance organic light emitting diodes, lasers and solar cells.[14] The benzofuro[2,3-*b*]carbazole core enhances the conjugation length, facilitating effective charge transfer and reducing recombination losses, which is essential for improving the PCE in OSCs. Furthermore, the incorporation of phenylsulfonyl groups contributes to electron-accepting properties, thus stabilizing the molecular structure and enhancing electron affinity. Their inclusion increases exciton dissociation efficiency and allows for better alignment with donor materials in bulk heterojunctions. The resulting extended absorption spectrum and tunable HOMO–LUMO energy levels support efficient light absorption and energy conversion in the visible range. Together, these structural and electronic characteristics make phenylsulfonyl-7*H*-benzofuro[2,3-*b*]carbazole-based materials versatile and promising components in high-performance OSCs, potentially advancing the efficiency and scalability of organic photovoltaics.[15]

In this study, a series of phenylsulfonyl carbazole-based derivatives (**PSCR** and **PSCD1–PSCD6**) with an A1–π–A2–π–A1 framework, was designed from a 12-methyl-7-(phenylsulfonyl)-7*H*-benzofuro[2,3-*b*]carbazole (PSC) core-based compound (**1**).[16] Structural tailoring was achieved by attaching one end of a thiophene π-spacer to the terminal of the phenylsulfonyl carbazole (PSC) acceptor (A2), while the other end π-spacer was connected to an indene malononitrile-based acceptor moiety (A1), as illustrated in Fig. 1. To understand their structure–property relationships, DFT was employed. This computational technique determines a system's geometry and ground-state characteristics on the basis of its electrical density.[17] It is anticipated that these designed derivatives might possess potential electronic and photovoltaic characteristics and could be used as candidate materials for OSCs.

Computational method

For the current investigation, a quantum chemical study was conducted with the aid of Gaussian 09 [18] software. To achieve this, the initial step was to optimize the geometries of **PSCR** and **PSCD1–PSCD6** using the M06 functional[19] with the 6-311G(d,p) basis set.[20] GaussView 6.0 [21] was used to visualize the results and draw the structures. Several electronic and photovoltaic properties, such as the density of states (DOS), UV-visible absorption spectra, reorganization energy (RE), global reactivity

descriptors, frontier molecular orbital (FMO)–based properties, non-covalent interactions (NCIs), exciton binding energy (E_b), transition density matrix (TDM), and open-circuit voltage (V_{oc}), were calculated using the optimized geometries of entitled compounds. Various software packages, including Avogadro,[22] Multiwfn,[23] Origin,[24] GaussSum,[25] PyMOlyze,[25] and Chemcraft,[26] were employed to analyze and interpret the data from output files. Reorganization energies for electrons (λ_e) and holes (λ_h) were determined using the following equations:

$$\lambda_e = [E_0^- - E_-] + [E_-^0 - E_0] \quad (1)$$

$$\lambda_h = [E_0^+ - E_+] + [E_+^0 - E_0]. \quad (2)$$

In these calculations, E_-^0 and E_+^0 represent the energies of the neutral molecule evaluated at the optimized geometries of the anion and cation, respectively; E_- and E_+ denote the energies of the anion and cation, correspondingly obtained from their optimized neutral molecule geomtery; E_0^- and E_0^+ are the single-point energies of the anion and cation, respectively, following optimization of their respective ions; and E_0 refers to the single-point energy of the neutral molecule in its ground state.

Results and discussion

In this study, organic chromophores (**PSCR** and **PSCD1–PSCD6**) were designed *via* structural modeling with the aim to enhance their photovoltaic performance. For this purpose, **PSCR** was employed as a reference compound, which was designed using the phenylsulfonyl carbazole (PSC) central acceptor moiety.[16] This core was linked to indene-based end-capped acceptor groups (2-(2-methylene-3-oxo-2,3-dihydro-1*H*-inden-1-ylidene) malononitrile) *via* a thiophene π-spacer. Six derivatives were designed by substituting different electron-withdrawing units, namely –F, –Cl, –CN, $-NO_2$, $-HSO_3$, and $-CF_3$, at the ends of 2-(2-methylene-3-oxo-2,3-dihydro-1*H*-inden-1-ylidene)malononitrile acceptor moieties to explore their impact on the photovoltaic properties of OSCs. Fig. 1 illustrates the strategy used to design these chromophores. Fig. S1† displays the chemical structures and Table S21† lists the IUPAC names of the designed compounds. The optimized geometries are displayed in Fig. S2,† while their ChemDraw structures are illustrated in Fig. S3.† Additionally, their Cartesian coordinates are provided in Tables S1–S7.†

Molecular geometric optimization and dihedral angles

The optimization of **PSCR** and **PSCD1–PSCD6** involved calculating their structural parameters, including bond lengths and dihedral angles. A comparison between the simulated and reported experimental geometries revealed good agreement, indicating the accuracy of the used computational procedure. For the compounds **PSCR** and **PSCD1–PSCD6**, the DFT-calculated C–C bond lengths in the benzene ring ranged from 1.388 to 1.457 Å, which were in close agreement with the reported bond lengths (1.267–1.345 Å) for a benzene ring.[27] The DFT-calculated bond length for the C–S bond in thiophene was 1.722 Å. Similarly, the C–N bond lengths in the terminal cyano groups of **PSCR** and **PSCD1–PSCD6** were calculated to be 1.155 Å in all the compounds. The simulated C–C–C bond angles within the benzene ring for **PSCR** and **PSCD1–PSCD6** were calculated as 113.3–128.3°, which were in agreement with the reported experimental values (121–141°).[27] Similarly, for the O=S=O bond angles in the phenylsulfonyl ring, the simulated bond angles were calculated as 122.5 Å. C–C–N bond angles were calculated to be in the range of 128.4–178.7° through DFT study. Further DFT-simulated bond lengths and bond angles are tabulated in Tables S14–S20.†

A dihedral angle is an angle formed between two planes that intersect along a shared bond, influencing the three-dimensional shape of a molecule. In organic chromophores, this angle significantly affects charge transfer. Furthermore, the dihedral angle is modified by the substituents linked to the molecular framework. Table S13† illustrates the dihedral angles (θ) of the studied chromophores (**PSCR** and **PSCD1–PSCD6**), while Fig. S1† shows the optimal geometries for all the compounds investigated. In this study, the values of the dihedral angle (θ_1 and θ_4) between the terminal acceptor (A1) and the π-spacers of the examined chromophores were found to be in the range of −174.26–2.760°, respectively. Similarly, the values of the (θ_2 and θ_3) dihedral angle between the π-spacers and the phenylsulfonyl carbazole central core (A2) of the studied chromophores **PSCR** and **PSCD1–PSCD6** ranged from 24.680° to −154.41°, as shown in Table S13.† The negative values of dihedral angles indicated the planar geometry of the title chromophores, suggesting good charge transfer (Fig. 2).

Electronic properties

Analysis of frontier molecular orbitals (FMOs) provides valuable insights into the optoelectronic properties. Furthermore, this analysis helps understand intermolecular charge transfer (ICT), chemical reactivity, dynamic stability and other aspects related to molecular interactions. E_{HOMO} and E_{LUMO} energies are significant quantum descriptors.[28] The band gap (E_g) help elucidate the increase and decrease in reactivity under the influence of various acceptor elements. Here, E_g represents the energy difference between the bonding and anti-bonding levels. The thiophene bridges play a vital role in facilitating the transfer of electron density from the core acceptor unit to terminal acceptor units.[29] These terminal electron-deficient units enhance the extent of conjugation and facilitate easier delocalization of the electronic cloud across the molecules. Additionally, the studied compounds exhibited rigid and planar structures, promoting strong intermolecular interactions and improved charge mobility. HOMO/LUMO band gaps results are provided in Table 1. Fig. 3 presents the molecular orbital diagrams for the reference and designed compounds. Additionally, Fig. S3† provides visual representations of HOMO − 1, LUMO + 1, HOMO − 2, and LUMO + 2 for all the designed compounds, while Table S8† presents the corresponding energy values.

The E_g for **PSCR** was calculated as 3.025 eV, with LUMO/HOMO energies of −3.381 and −6.406 eV, respectively. **PSCD1–PSCD6** chromophores showed comparable E_g values (2.742–

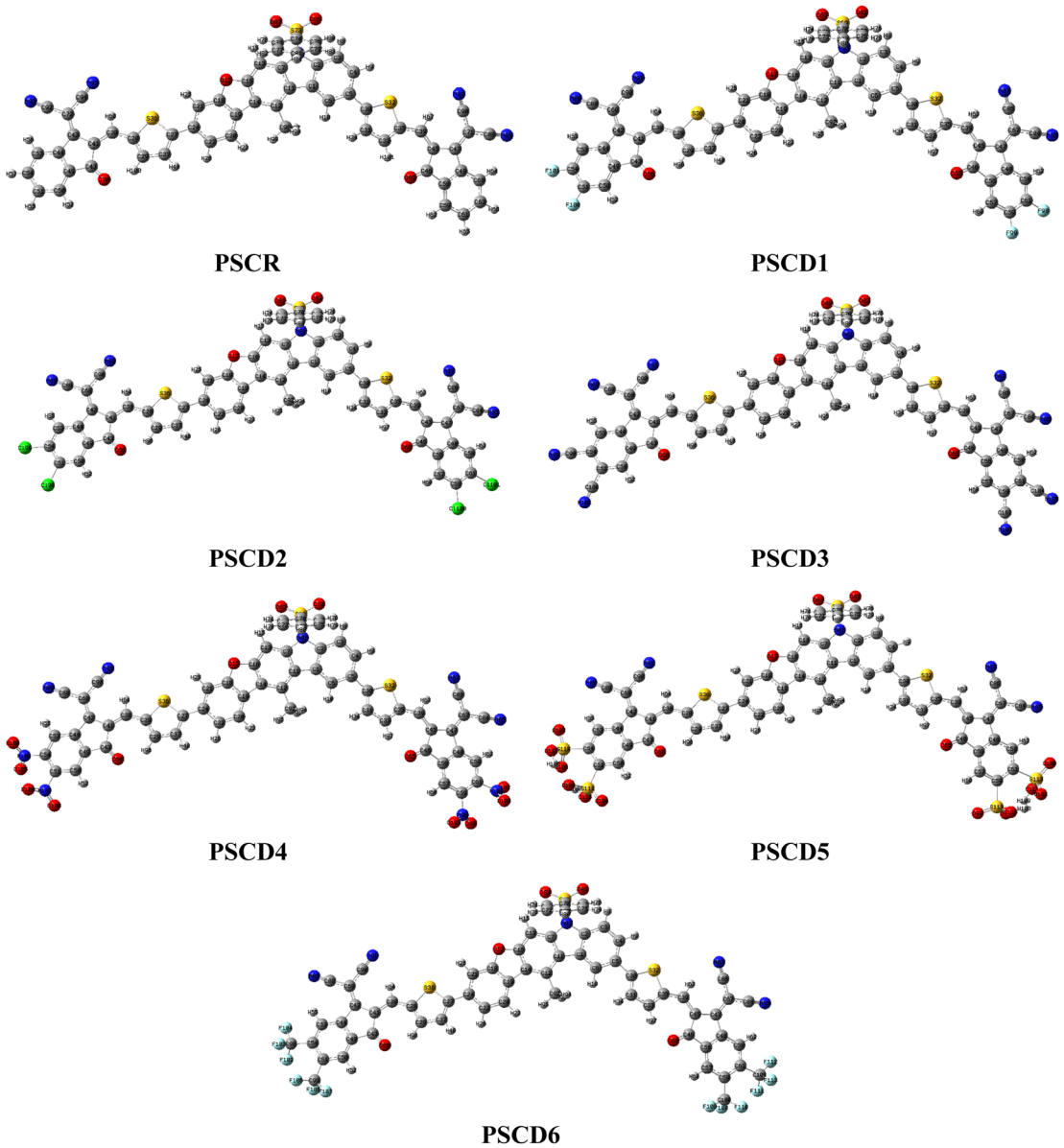

Fig. 2 Optimized structures of the designed chromophores (PSCR and PSCD1–PSCD6).

Table 1 Frontier molecular orbital energies of PSCR and PSCD1–PSCD6; units are given in eV

Compounds	E_{HOMO}	E_{LUMO}	E_{gap}
PSCR	−6.406	−3.381	3.025
PSCD1	−6.530	−3.552	2.978
PSCD2	−6.545	−3.599	2.946
PSCD3	−6.817	−4.039	2.778
PSCD4	−6.828	−4.086	2.742
PSCD5	−6.814	−4.045	2.769
PSCD6	−6.682	−3.808	2.874

2.978 eV) to **PSCR**. Furthermore, the calculated HOMO energies of **PSCD1–PSCD6** were obtained as −6.406, −6.530, −6.545, −6.682, −6.814, −6.817 and −6.828 eV, respectively whereas the LUMO energies of these molecules were −3.381, −3.552, −3.599, −3.808, −4.039, −4.045 and −4.086 eV, correspondingly. Among all the designed chromophores, **PSCD4** exhibited the smallest band gap at 2.742 eV. This could likely be attributed to the powerful electron-withdrawing behavior of the nitro (–NO_2) groups attached to the terminal acceptor moieties of 2-(2-methylene-3-oxo-2,3-dihydro-1*H*-inden-1-ylidene)malononitrile. The –NO_2 group displays strong resonance, facilitate efficient charge transfer due to its unpaired electrons, and has a negative inductive effect (−*I*). This promotes the transfer of charge density from the HOMO of the π-bridge to the LUMO of the acceptor fragment in **PSCD4**.[30]

The derivatives **PSCD1** and **PSCD2** displayed similar band gaps of 2.978 and 2.946 eV, respectively. The –Cl group in **PSCD1** exhibited a weaker −*I* effect compared with the –F group in

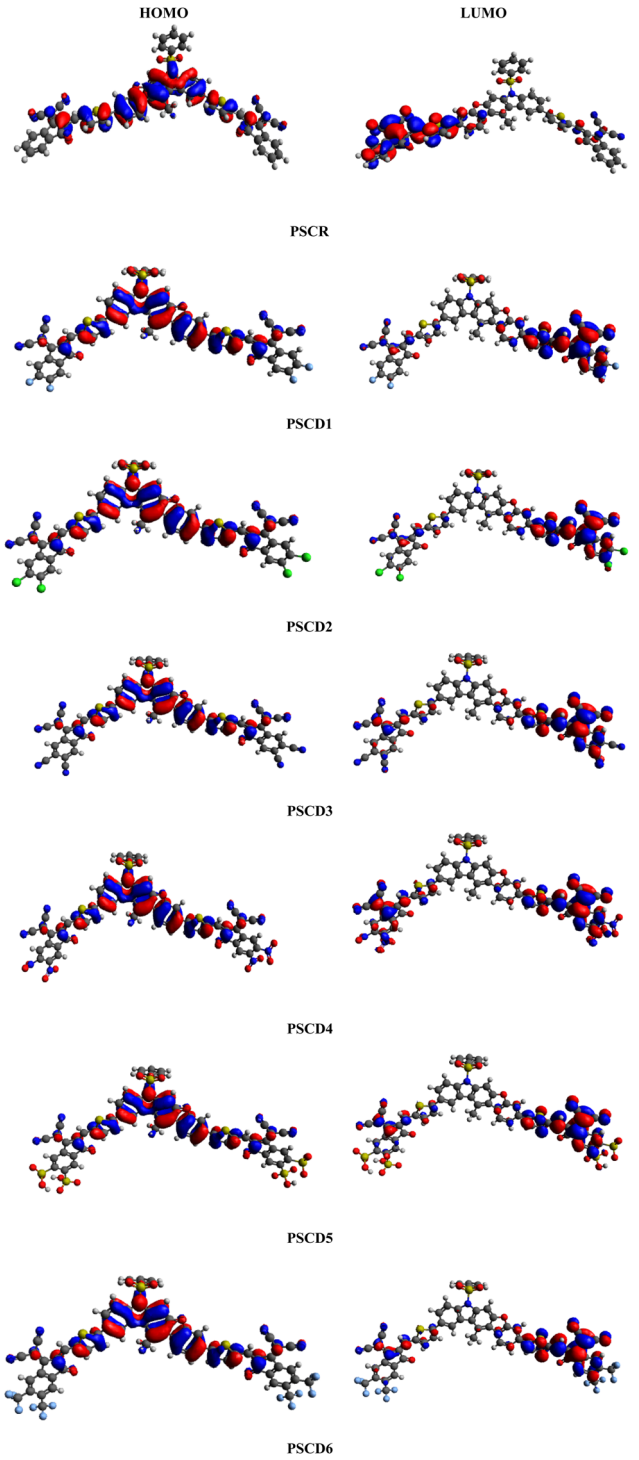

Fig. 3 Schematic of the FMOs of PSCR and PSCD1–PSCD6 illustrating the charge density on the orbitals.

PSCD2 as fluorine is more electronegative than chlorine; therefore, a reduction in the E_g of **PSCD1** was found. Consequently, the second narrowest band gap was observed in **PSCD3** (2.778 eV) and **PSCD5** (2.769 eV), likely owing to effective electron-withdrawing substituents –CN and $-SO_3H$ at the terminal end of the acceptor, respectively. The –CN and $-SO_3H$ groups attract electrons toward themselves, enhancing the efficiency of electronic charge delocalization within compounds. This leads to extended conjugation and increased charge-carrier mobility. A higher E_g of 2.874 eV was observed in the **PSCD6** compound among all the derivatives, because of the introduction of the $-CF_3$ group in the terminal acceptor unit of 2-(2-methylene-3-oxo-2,3-dihydro-1*H*-inden-1-ylidene)malononitrile. The overall decreasing order of E_g in eV was as follows: **PSCR** (3.025) > **PSCD1** (2.978) > **PSCD2** (2.946) > **PSCD6** (2.874) > **PSCD3** (2.778) > **PSCD5** (2.769) > **PSCD4** (2.742). The density of charges in HOMO was spread on the bridge units, while in LUMO, it was positioned on the acceptor moieties, as indicated by the FMO surfaces of the designated compounds. In the title chromophores, the effective charge transfer suggests these chromophores could be suitable OSC candidates.

Density of states (DOS)

The DOS represents the distribution of the accessible electronic state that electrons can occupy at a specific energy level. Moreover, DOS analysis is crucial for determining the electron-transition rate in molecules.[31] Thus, DOS analysis can help validate FMO results and quantify the contribution of HOMO (valence band) and LUMO (conduction band) to charge densities. A DOS plot illustrates the electron distribution across the molecules and indicates the number of positions occupied by electrons at band structures (HOMO and LUMO energy levels). Additionally, it reveals the contribution of each fragment to the formation of HOMO and LUMO.[32] In this investigation, the molecules were divided into three fragments: end-capped acceptors (A1), a π-linker, and a core unit (A2). The graphical representations of the DOS analysis are provided in Fig. 4. In Fig. 4, the peaks on the left side of the graph between −6.5 and −16 are HOMOs (HOMO, HOMO − 1 and HOMO − 2, *etc.*), while the peaks on the left side of the map are the LUMOs (LUMO, LUMO + 1 and LUMO + 2, *etc.*). The black peaks in Fig. 4 show the overall density of electrons at the energy levels of both fragments. The green color represents the electron density at the π-spacer of the chromophore, whereas the red and blue peaks correspond to the acceptor region. The Fermi level shows a significant role in determining the electronic behavior of materials. It represents the energy level at which the probability of electron occupancy is 50% at absolute zero and serves as a reference point separating occupied states (below the Fermi level) from unoccupied states (above the Fermi level). In intrinsic semiconductors, the Fermi level lies midway between the valence and conduction bands, whereas in doped semiconductors, it is shifted closer to the conduction band (n-type) or the valence band (p-type).[32] As the current studied compounds were n-type semiconductors, the Fermi level moved toward the conduction band, as illustrated in Fig. 4.

Table S11† shows the charge distribution pattern for the terminal acceptors (A1), contributing 14.0%, 16.5%, 16.7%, 16.9%, 17.4%, 18.0%, and 19.3% to HOMO, and 15.5%, 68.5%, 69.3%, 71.6%, 75.3%, 76.1%, and 78.6% to the LUMO for **PSCR** and **PSCD1–PSCD6**, respectively. Similarly, the π-spacer contributed 1.3%, 20.4%, 20.5%, 20.8%, 22.1%, 24.1%, and 25.5% to HOMO, and 7.0%, 15.9%, 18.0%, 18.7%, 21.2%,

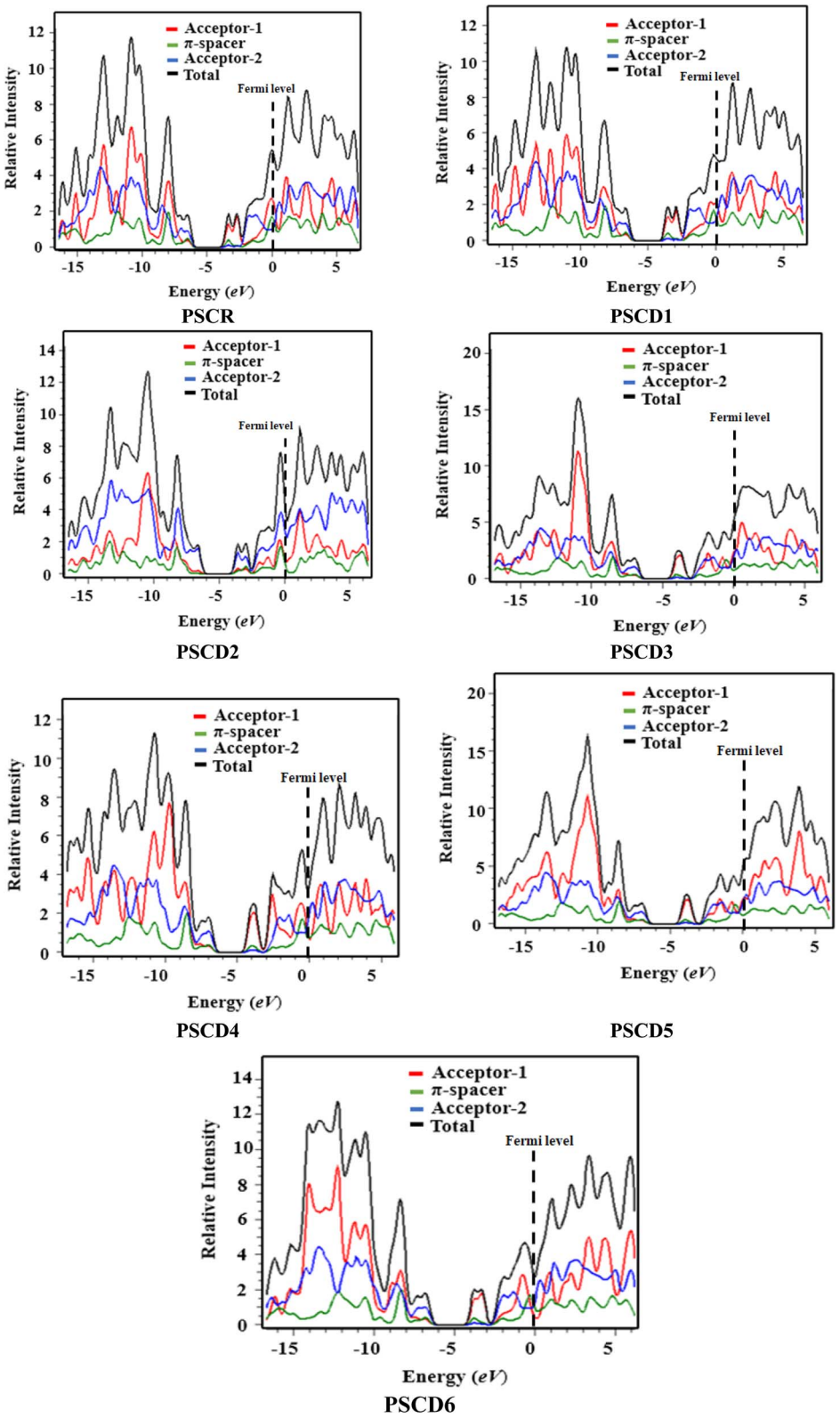

Fig. 4 DOS plots for PSCR and PSCD1–PSCD6.

22.7%, and 23.1% to LUMO for all the examined compounds, respectively. Likewise, A2 contributed 55.2%, 57.9%, 60.5%, 62.3%, 62.8%, 63.1%, and 84.7% to HOMO, and 5.4%, 5.8%, 6.0%, 7.1%, 8.0%, 8.5%, and 77.5% to LUMO for the studied organic chromophores. In the valence band of all the chromophores, the electronic cloud was mostly concentrated on the

linker and in conduction band this charge moved toward the terminals (acceptors).

Global reactivity parameters (GRPs)

The band gap determined on the basis of FMOs is essential for calculating GRPs of the designed compounds. Moreover, GRPs for the designed compounds (**PSCR** and **PSCD1–PSCD6**) were calculated using Koopmans' theorem.[33] These parameters include the ionization potential (IP),[34] electron affinity (EA),[35] electronegativity (X),[36] global softness (σ),[37] hardness (η),[38] global electrophilicity index (ω),[39] chemical potential (μ),[40] and charge transfer within a molecule (ΔN_{max}).[41] Equations in Table S22† assisted in the theoretical calculations of GRPs for the studied compounds.

Table 2 presents the calculated GRP values for **PSCR** and **PSCD1–PSCD6**. Efficient charge transfer depends on the molecules' IP and EA. The IP denotes the energy needed to lose an electron from the outermost shell,[42] while EA represents the amount of energy emitted when a molecule gains an electron. From Table 2, it is evident that all the designed compounds exhibited high values of electron affinity and ionization potential, which supports the elevated LUMO levels in these compounds. The calculated ionization potential (IP) values in descending order were **PSCD4** (6.828 eV) > **PSCD3** (6.817 eV) > **PSCD5** (6.814 eV) > **PSCD6** (6.682 eV) > **PSCD2** (6.545 eV) > **PSCD1** (6.530 eV) > **PSCR** (6.406 eV). Conversely, a molecule with a shorter energy gap is considered softer, indicating increased reactivity and poorer stability.

Global softness values in descending order were **PSCD4** ($0.364\ eV^{-1}$) > **PSCD5** ($0.361\ eV^{-1}$) > **PSCD3** ($0.359\ eV^{-1}$) > **PSCD6** ($0.340\ eV^{-1}$) > **PSCD2** ($0.339\ eV^{-1}$) > **PSCD1** ($0.335\ eV^{-1}$) > **PSCR** ($0.330\ eV^{-1}$).

Among all the chromophores studied, **PSCD4** was the most electronegative, with an electronegativity value of 5.457. Additionally, its strong acceptor nature was confirmed by a low chemical potential (μ) value of −5.457, highlighting its enhanced charge-transfer (CT) capabilities. Reactivity depends on η and σ, which are essential characteristics that are inversely proportional. Molecules with greater σ and lower η values display the shortest HOMO–LUMO energy gap, reduced stability, and enhanced reactivity.[43] Remarkably, **PSCD4** showed the maximum σ value of $0.364\ eV^{-1}$ among the above-mentioned chromophores. Conversely, the minimum η value for **PSCD4** was 1.094 eV. Furthermore, **PSCD4** exhibited the highest ΔN_{max} at 3.980 eV. All the designed molecules showed higher softness and lower hardness values, indicating their high polarizability.

UV-visible analysis

UV-visible study is crucial for analyzing electronic transitions and identifying the configurations that contribute to them.[44] The simulated UV-vis absorption properties of the titled chromophores were estimated in the gaseous phase. Additional values for the individual compounds are provided in Table S9.† Table S10† provides further detailed information, including the transition energy from the ground state (S_0) to the first excited state (S_1) (denoted as E_{opt}), the maximum absorption wavelength (λ_{max}), the oscillator strength (f_{os}) at λ_{max}, and an analysis of the molecular orbital contributions and transition characteristics for the transition from S_0 to S_1. Fig. S4† depicts the UV-visible spectra for the designated chromophores. All the titled chromophores exhibited UV-visible spectra in the 496.891–545.009 nm range. However, the designed chromophores (**PSCD1–PSCD6**) demonstrated significant bathochromic shifts and lower excitation energy values compared with the reference compound **PSCR**. Typically, a red-shift in the absorbance spectra leads to enhanced electron mobility.

In the gaseous phase, **PSCR** showed $\lambda_{max} = 496.891$ nm with an E of 2.495 eV at $2.298\ f_{os}$. **PSCD1–PSCD6** exhibited λ_{max} values of 504.452, 511.085, 522.083, 539.531, 541.321, and 545.009 nm, respectively. Correspondingly, they displayed lower E values of 2.458, 2.426, 2.375, 2.298, 2.290, and 2.275 eV. Moreover, their f_{os} values were 2.289, 2.219, 2.132, 1.983, 1.921, and 1.726. Overall, all the compounds showed red shift in absorption maximum (λ_{max}) in the following ascending order: **PSCR** < **PSCD1** < **PSCD2** < **PSCD6** < **PSCD3** < **PSCD5** < **PSCD4**. These results reveal that **PSCD4** exhibited the highest red-shifted values for absorption compared with the other derivatives.

Reorganization energy (RE)

The RE is a fundamental parameter in understanding the efficacy of a solar cell as it is closely linked to its charge-transfer (CT) capability. The charge-transfer phenomenon in BHJ-OSCs is governed by Marcus theory, which establishes a relationship between the RE and the charge-transfer rate (k), as presented in eqn (3):

$$k = \frac{2\pi}{h\sqrt{4\pi\lambda k_B T}} V^2 \exp\left[-\frac{(\lambda + \Delta G)^2}{4\pi k_B}\right]. \quad (3)$$

Table 2 Computed GRPs of the title chromophores; $\sigma = eV^{-1}$ while all other units are in eV

Compounds	X	μ	η	σ	ω	IP	EA	ΔN_{max}
PSCR	4.893	−4.983	1.512	0.330	7.916	6.406	3.381	3.295
PSCD1	5.041	−5.041	1.489	0.335	8.533	6.530	3.552	3.385
PSCD2	5.072	−5.072	1.473	0.339	8.732	6.545	3.599	3.443
PSCD3	5.428	−5.428	1.389	0.359	10.605	6.817	4.039	3.385
PSCD4	5.457	−5.457	1.371	0.364	10.860	6.828	4.086	3.980
PSCD5	5.429	−5.429	1.384	0.361	10.646	6.814	4.045	3.922
PSCD6	5.245	−5.245	1.437	0.340	9.572	6.682	3.808	3.649

Here, k_B represents the Boltzmann constant, T denotes temperature, ΔG indicates the Gibbs free energy, and V refers to the electronic coupling between the final and initial states. According to Marcus theory, a lower RE is correlated with enhanced CT efficiency, facilitating improved photovoltaic properties. The RE can be distributed into two primary components: external RE (λ_{ext}) and internal RE (λ_{int}),[45] where λ_{ext} pertains to the relaxation of the surrounding environment, while the λ_{int} refers to rapid structural changes within the molecule itself. In OSCs, charge-carrier mobility is primarily governed through identical or nearly identical sites, where free energy changes can typically be neglected.[46] In this study, λ_{int} values for holes and electrons were calculated for **PSCD1–PSCD6** molecules, as shown in Table S23.† The calculated RE (λ_h) values for the holes in **PSCD1–PSCD6** were −0.00027591, −0.00007466, −0.00029709, −0.00585749, and 0.00019163 eV, respectively. Similarly, the computed (λ_e) values for the electrons in **PSCD1–PSCD6** were 0.00034201, 0.00034764, 0.00038431, 0.00011124, and 0.00011465 eV, respectively. The descending order of λ_e for these compounds was **PSCD4** > **PSCD2** > **PSCD1** > **PSCD6** > **PSCD5**. Molecules with lower λ_e values can serve as more effective acceptor moieties by facilitating electron transfer from the donor core to the terminal acceptor. RE (λ_e) values indicated that compounds **PSCD4** and **PSCD5** exhibited significantly lower values compared with the others, aligning with Marcus theory by implying their more efficient electron transfer due to their reduced energy barriers. This makes them strong candidates as electron acceptor materials, as a lower λ_e promotes faster and more effective electron hopping. In contrast, the hole reorganization energy (λ_h) displayed a wider range of values for the compounds. Notably, **PSCD1–PSCD4** exhibited negative λ_h values, whereas **PSCR** and **PSC5** exhibited positive λ_h values, which suggested stable hole-transfer processes. According to Marcus theory, the balance among λ, ΔG, and V is crucial for maximizing the charge-transfer rate, and these compounds demonstrated favorable conditions for hole transport. The electron–hole indices of **PSCR–PSCD6** shown in Table S24† illustrate a lower range of excitation energy, specifically between 2.275 and 2.495 eV, indicating UV-vis absorption. The D index, a measure used in determining the spatial separation between holes and electrons, showed a modest 2.709–4.317 Å range when the dispersal of electrons and electrons was examined. This suggests that the spreading of charges was optimally separate. **PSCD1** exhibited the highest coulombic attraction energy (E_{Coul}), at 2.1833 eV, while **PSCD4** exhibited the lowest value, at 1.8473 eV. The compounds with E_{Coul} in ascending order are given as follows: **PSCD1** > **PSCD2** > **PSCD6** > **PSCD3** > **PSCD5** > **PSCD4**. There was a wide distribution of electrons and holes, with higher values representing charge distribution, according to the H indices—a metric that characterizes the amount of overlap between the electron and hole distributions inside a molecule during electron excitation. Further, all the compounds had high values (>0.4) of the Sr index—a measure of the spatial gap between holes and electrons, which suggests the occurrence of π–π* transitions. The title compounds showed Sr values between 0.4540 and 0.5765, *i.e.*, all below 1, indicating a large overlap between electrons and holes that favors efficient charge transit in the chromophores. Overall, the findings demonstrate that the designed chromophores exhibited lower REs, which suggests that they are good candidates for efficient charge transfer.

Transition density matrix (TDM) investigations

The TDM is important for analyzing the electronic excitations and CT phenomenon within a molecule. Additionally, it aids in understanding the interactions amid donor and acceptor components, the overlap between holes and electrons, and the extent of ICT.[46] The TDM analyzes electronic excitations, from S_0 to S_1, and the extent of delocalization within molecules.[47] Owing to the minor contribution of H atoms, they are neglected in this analysis. TDM plots for **PSCD1–PSCD6** are presented in Fig. 5, with the electron cloud depicted in green, yellow and red colors against a dark background.

PSCD1–PSCD6 were divided into three parts, as shown in Fig. 1: A1, A2, and the π-linker. **PSCR** and **PSCD1–PSCD6** displayed charge transfer from A2 to the terminal moiety (A1). The π-linker unit helps with this procedure without creating any hindrance.

The electronic cloud was predominantly concentrated on the A2 entity, relatively distributed across the π-linker, and minimally localized on the terminal A1 moieties. Additionally, extensive charge dispersion occurred along the diagonal routes. Consequently, all the title compounds exhibited significantly greater charge dissociation and low coulombic interactions, which indicated their potential utilization as photovoltaic materials.

Exciton binding energy (E_b)

The least energy needed to separate a free electron and hole after their formation as an electron–hole pair, upon absorbing solar radiation, is known as the binding energy (E_b).[48] A lower binding energy results in easier separation of holes and electrons from excitons, allowing charges to reach their respective electrodes more efficiently, thereby increasing the current yield.[49] The binding energy value is influenced by the acceptor subunits attached to a molecule's peripheries. Highly electronegative or strong electron-withdrawing groups lower the binding energy by weakening the coulombic force between electrons and holes, as they strongly attract electrons towards themselves.[50] The binding energy can be calculated using eqn (4):

$$E_b = E_{H-L} - E_{opt}, \quad (4)$$

where E_b represents the binding energy of the electron–hole pair, E_{H-L} is the band gap between the HOMO and LUMO of the studied molecules, and E_{opt} characterizes the first excitation energy of an electron in the molecules. The energy gap refers to the energy required to generate an unbound charge carrier, such as an electron or hole. Through subtracting the S_1 energy from the E_g, the remaining energy corresponds to the formation of an exciton, which is a bound state consisting of an electron–hole pair. The E_b values of **PSCR** and **PSCD1–PSCD6** are provided in Table 3.

All the designed compounds showed an improved charge-separation ability because of their low E_b values. Specifically, the E_b values of **PSCR** and **PSCD1–PSCD6** were 0.530, 0.520,

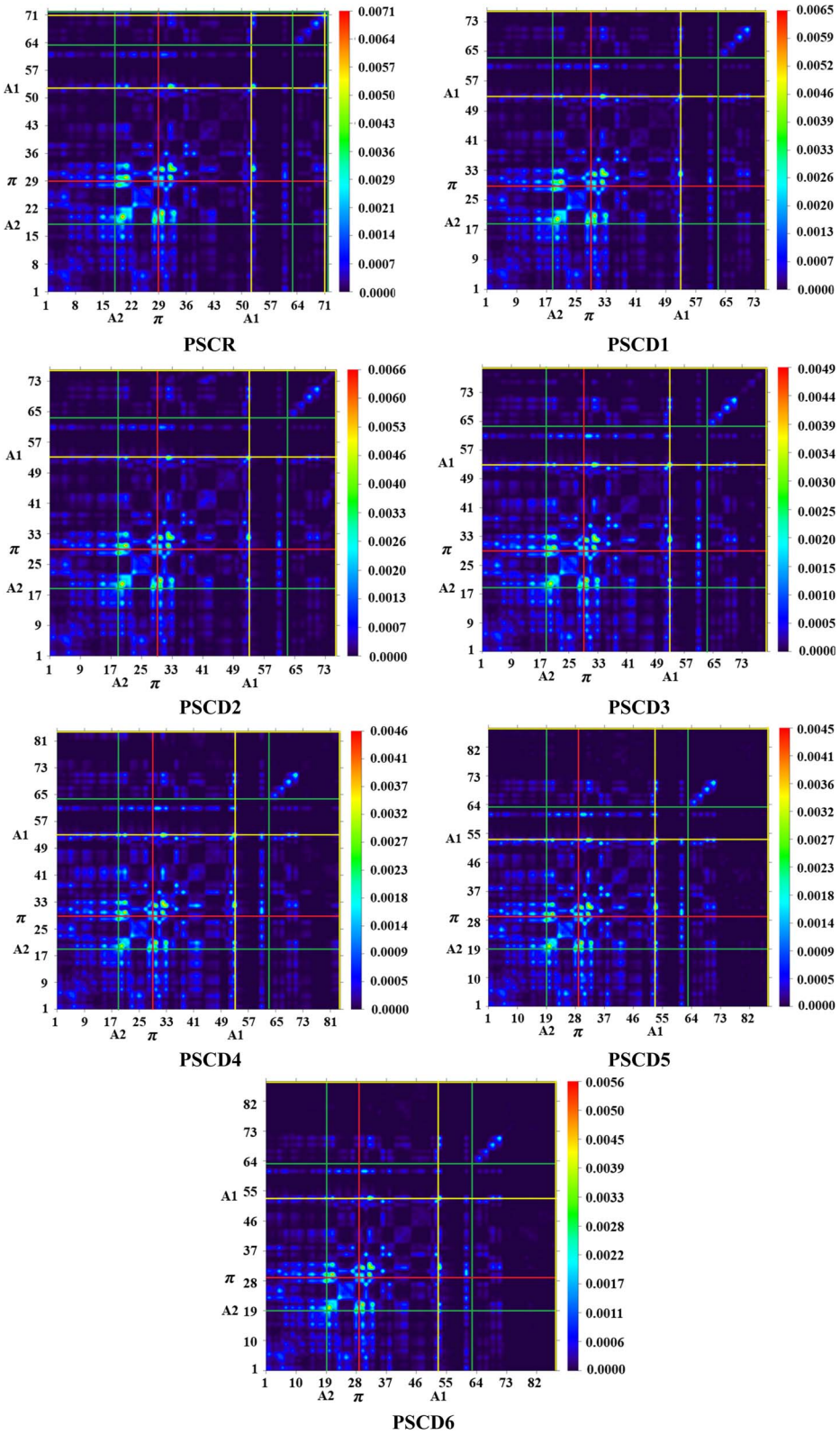

Fig. 5 Transition density matrix maps of PSCR and PSCD1–PSCD6.

0.520, 0.480, 0.467, 0.479, and 0.499 eV, respectively. The increasing trend of E_b for all the examined compounds was as follows: **PSCD4 < PSCD5 < PSCD3 < PSCD6 < PSCD1 = PSCD2 < PSCR.** Chromophores with a low E_b, allowing easier exciton dissociation and rapid charge flow, show enhanced current density, making them extremely appropriate for optoelectronic applications.[51] All the title compounds in the present study had E_b values < 1.9 eV, making them suitable for optical activity and

Table 3 Calculated binding energies (E_b) of the title compounds; units are given in eV

Compounds	E_{H-L}	E_{opt}	E_b
PSCR	3.025	2.495	0.530
PSCD1	2.978	2.458	0.520
PSCD2	2.946	2.426	0.520
PSCD3	2.778	2.298	0.480
PSCD4	2.742	2.275	0.467
PSCD5	2.769	2.290	0.479
PSCD6	2.874	2.375	0.499

a variety of OSC applications. Among all the designed compounds, **PSCD4** exhibited the lowest binding energy value (0.467 eV), indicating its excellent optoelectronic properties with significant dissociation of excitons in the S_1.

Photovoltaic properties

V_{oc} signifies the highest voltage a solar cell can generate under open-circuit conditions, when there is no current flow, with minimal external influence.[52] V_{oc} is a key factor in evaluating the PCE of OSCs.[53] Fig. 6 illustrates a graphical representation of the V_{oc} values for **PSCR** and **PSCD1–PSCD6** in conjunction with **PBDBT**. The theoretical V_{oc} values for **PSCR** and **PSCD1–PSCD6** are calculated using the Scharber equation[54] (eqn (5)):

$$V_{oc} = \frac{1}{e}\left(\left|E^{D}_{HOMO}\right| - \left|E^{A}_{LUMO}\right|\right) - 0.3. \quad (5)$$

All the designed molecules (**PSCR** and **PSCD1–PSCD6**) demonstrated significant V_{oc} values, as indicated in Table S12.† The E_{HOMO} of **PBDBT** was −5.401 eV and E_{LUMO} was −2.328 eV. The V_{oc} values of **PSCR** and **PSCD1–PSCD6** were as follows: **PSCR** (1.720 V), **PSCD1** (1.549 V), **PSCD2** (1.502 V), **PSCD3** (1.062 V), **PSCD4** (1.015 V), **PSCD5** (1.056 V), and **PSCD6** (1.293 V). These significant findings might be attributed to the terminal group alteration with efficient acceptors. The reducing order of V_{oc} for the title chromophores was **PSCR** > **PSCD1** > **PSCD2** > **PSCD6** > **PSCD3** > **PSCD5** > **PSCD4**. The predicted theoretical results of V_{oc} reflect the efficacy of the structural modeling for enhancing the photovoltaic characteristics of the designed compounds. Literature studies reveal that the experimental-based V_{oc} values of OSCs can be found up to 0.98 V.[55] However, the calculated V_{oc} values for the reported chromophores were found to be in the range of 1.015–1.720 V. This difference might be due to the fact that the DFT/TD-DFT investigations were performed on isolated molecules in the gaseous phase. Furthermore, experimental findings might be influenced by molecular packing, charge recombination, and other complex material interactions.

Fill factor (FF) and power conversion efficiency (PCE)

The FF is another crucial determinant of the PCE of OSCs. The FF values for **PSCR** and **PSCD1–PSCD6** were calculated with the aid of eqn (6)[55] and the results are reported in Table S12.†

$$FF = \frac{\frac{eV_{oc}}{KBT} - \ln\left[\frac{eV_{oc}}{KBT} + 0.72\right]}{\frac{eV_{oc}}{KBT} + 1} \quad (6)$$

The equation $\frac{eV_{oc}}{KBT}$ represents normalized V_{oc}, which is an important factor calculated at standard room temperature under neutral charge conditions in molecules.[56] This value is used instead of V_{oc} in FF calculations for greater accuracy. All the newly designed molecules exhibited FF values within an optimal range, suggesting their potential effectiveness in OSC applications. Similarly, another important factor is PCE, which can be calculated using eqn (7).[57]

$$PCE = \frac{J_{sc}V_{oc}FF}{P_{in}} \quad (7)$$

The PCE is utilized to estimate the efficacy of OSCs. The open-circuit voltage (V_{oc}), short-circuit current density (J_{SC}), incident light power (P_{in}), and fill factor (FF) are proportional to PCE. The PCE of the reported chromophores falls in the range of 13.92–24.17%, as indicated in Table S12.†

Non-covalent interactions (NCIs) analysis

The study of NCIs represents a significant advancement in molecular research, providing critical insights into electron density and non-covalent interactions, including hydrogen bonding, halogen bonding, and π–π stacking.[58] A quantitative measure of non-covalent interactions is derived by analyzing the

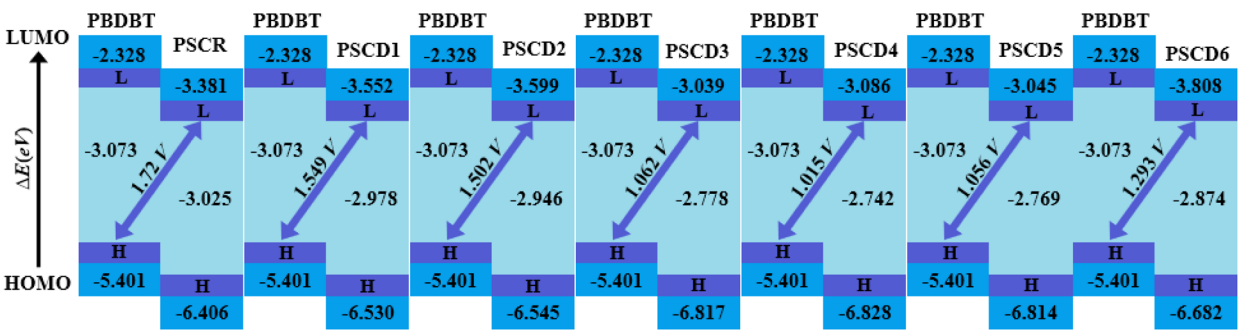

Fig. 6 Open-circuit voltage (V_{oc}) maps of the title chromophores with respect to **PBDBT**.

reduced density gradient (s) and the Laplacian of the electron density at zero-gradient sites.[59] This index can be depicted in two or three dimensions, illustrating the decreased density gradient (s) alongside the product of the electron density and the sign of λ_2, which is an eigenvalue of the electron density Hessian matrix.[60] The resultant plot exhibits significant spikes in areas of low electron density (ρ) and a diminished gradient, with an increased interface strength, signified by larger departures of spike amplitudes from zero. The λ_2 sign is essential for analyzing NCIs: negative λ_2 values indicate attractive interactions, whilst positive values signify repulsive forces, offering comprehensive insights into the characteristics of these interactions.

To aid comprehension, these interactions are represented in three dimensions using the NCI isosurface (ρ). Additionally, a two-dimensional graphical depiction of the reduced density gradient (RDG), generated using Multiwfn 3.7 software, is applied to discriminate between interface types that include hydrogen bonding, van der Waals forces, and steric effects. Fig. S5† presents $\lambda_2\rho$ plots alongside the corresponding NCI isosurfaces, highlighting the interactions for **PSCR** and **PSCD1–PSCD6** in chloroform, calculated at the M06/6-311G(d,p) level. The visualization incorporated scatter plots and RDG isosurfaces, with appealing interactions displayed in blue, van der Waals forces in green, and strong repellent interactions (steric effects) in red for all the designed derivatives. In the spectra, the x-axis represents the electron density as the product of λ_2 and ρ, while the y-axis denotes the reduced density gradient. Spikes at the extremes of the plots are particularly notable, with the left spike with values approaching approximately −0.05 a.u., indicating strong attractive interactions, whereas the right spike, nearing 0.05 a.u., reflects strong repulsive interactions. Furthermore, in these presented plots, the higher position of the blue band compared with the red band indicates a prevalence of attractive interactions. This dominance of attractive forces plays a key role in enhancing molecular stability. In conclusion, this research stresses the critical significance of attractive interactions, especially hydrogen bonding, in regulating the stability and photovoltaic properties of the reported **PSCD1–PSCD6** derivatives.

Conclusion

In summary, the organic chromophores **PSCR** and **PSCD1–PSCD6** were designed using end-capped modifications to obtain potential photovoltaic materials. The structural modifications of the terminal acceptors incorporating various electron-withdrawing groups resulted in higher bathochromic shifts and reduced energy gaps. Quantum chemical calculations were performed to investigate the optoelectronic characteristics of the title compounds. Among all the derivatives, **PSCD4** displayed the lowest E_g (2.742 eV), the widest absorption spectrum (545.009 nm), and the lowest binding energy value (0.467) owing to the introduction of the $-NO_2$ moiety at the end of the acceptor. RE and TDM results indicated that exciton dissociation occurred with significant charge transfer in all the derivatives. Moreover, the studied compounds were blended with the donor polymer **PBDBT** to determine their photovoltaic potential and good V_{oc}, FF, and PCE values were determined. These findings indicate that by employing structural modeling with efficient electron-withdrawing terminal acceptors, desired photovoltaic materials can be designed.

Data availability

All data generated or analyzed during this study are included in this published article and its ESI files.†

Conflicts of interest

There are no conflicts of interest to declare.

Acknowledgements

Dr Muhammad Khalid gratefully acknowledges the financial support of HEC Pakistan (project no. 20-14703/NRPU/R&D/HEC/2021). A. A. C. B. acknowledges the financial support of the São Paulo Research Foundation (FAPESP) (grants 2014/25770-6 and 2015/01491-3), the Conselho Nacional de Desenvolvimento Científico e Tecnológico (CNPq) of Brazil for academic support (grant 309715/2017-2), and Coordenação de Aperfeiçoamento de Pessoal de Nível Superior (CAPES), Brazil, that partially supported this work (Finance Code 001). The authors thank the Researchers Supporting Project number (RSPD2025R645), King Saud University, Riyadh, Saudi Arabia.

References

1 M. Irfan, R. M. Elavarasan, Y. Hao, M. Feng and D. Sailan, *J. Cleaner Prod.*, 2021, **292**, 126008.
2 M. Tawalbeh, A. Al-Othman, F. Kafiah, E. Abdelsalam, F. Almomani and M. Alkasrawi, *Sci. Total Environ.*, 2021, **759**, 143528.
3 M. Riede, D. Spoltore and K. Leo, *Adv. Energy Mater.*, 2021, **11**, 2002653.
4 J. Zhao, Y. Li, G. Yang, K. Jiang, H. Lin, H. Ade, W. Ma and H. Yan, *Nat. Energy*, 2016, **1**, 1–7.
5 W. Huang, P. Cheng, Y. Yang, G. Li and Y. Yang, *Adv. Mater.*, 2018, **30**, 1705706.
6 K. Atiq, M. M. A. Iqbal, T. Hassan and R. Hussain, *J. Mol. Model.*, 2024, **30**, 13.
7 C. Coluccini, P. T. Anusha, H.-Y. T. Chen, S.-L. Liao, Y. K. Ko, A. Yabushita, C. W. Luo, Y. M. Ng and Y. L. Khung, *Sci. Rep.*, 2019, **9**, 12762.
8 Y. Tong, Z. Xiao, X. Du, C. Zuo, Y. Li, M. Lv, Y. Yuan, C. Yi, F. Hao and Y. Hua, *Sci. China: Chem.*, 2020, **63**, 758–765.
9 Y. Liang, Z. Xu, J. Xia, S.-T. Tsai, Y. Wu, G. Li, C. Ray and L. Yu, *Adv. Mater.*, 2010, **22**, E135.
10 Y. Lin, Q. He, F. Zhao, L. Huo, J. Mai, X. Lu, C.-J. Su, T. Li, J. Wang and J. Zhu, *J. Am. Chem. Soc.*, 2016, **138**, 2973–2976.
11 Y. Zhang, Z. Liu, T. Shan, Y. Wang, L. Zhu, T. Li, F. Liu and H. Zhong, *Mater. Chem. Front.*, 2020, **4**, 2462–2471.
12 M. Muppuli, K. Rajesh, D. Anitha Rexalin, K. Anandan, K. Gayathri, A. Mani, P. Devendran, V. Thayanithi, P. Kurinjinathan and M. Suresh Kumar, *J. Struct. Chem.*, 2024, **65**, 987–1001.

13 A. van Dijken, J. J. Bastiaansen, N. M. Kiggen, B. M. Langeveld, C. Rothe, A. Monkman, I. Bach, P. Stössel and K. Brunner, *J. Am. Chem. Soc.*, 2004, **126**, 7718–7727.
14 D. Avcı, S. Altürk, F. Sönmez, Ö. Tamer, A. Başoğlu, Y. Atalay, B. Zengin Kurt, D. Öztürk and N. Dege, *Appl. Organomet. Chem.*, 2019, **33**, e4725.
15 K. Lupinska, S. Kotowicz, A. Grabarz, M. Siwy, K. Sulowska, S. Mackowski, L. Bu, Y. Bretonnière, C. Andraud, E. Schab-Balcerzak and L. Sznitko, *ACS Omega*, 2024, **9**, 40769–40782.
16 R. Gangadharan, P. Narayanan, K. Sethusankar, V. Saravanan and A. K. Mohanakrishnan, *Acta Crystallogr., Sect. E: Struct. Rep. Online*, 2016, **72**, 1744–1750.
17 R. D. Mills-Williams, B. D. Goddard and A. J. Archer, *J. Chem. Phys.*, 2024, **160**, 174901.
18 M. J. Frisch, G. W. Trucks, H. B. Schlegel, G. E. Scuseria, M. A. Robb, J. R. Cheeseman, G. Scalmani, V. Barone, B. Mennucci and G. A. Petersson, *Gaussian 09, Revision A. 02*, Gaussian Inc., Wallingford CT, 2016.
19 Y. Zhao and D. G. Truhlar, *Theor. Chem. Acc.*, 2008, **120**, 215–241.
20 J. E. Del Bene, D. H. Aue and I. Shavitt, *J. Am. Chem. Soc.*, 1992, **114**, 1631–1640.
21 R. Dennington, T. A. Keith and J. M. Millam, *GaussView 5.0*, Gaussian Inc., Wallingford, 2008, p. 20.
22 M. D. Hanwell, D. E. Curtis, D. C. Lonie, T. Vandermeersch, E. Zurek and G. R. Hutchison, *J. Cheminf.*, 2012, **4**, 1–17.
23 T. Lu and F. Chen, *J. Comput. Chem.*, 2012, **33**, 580–592.
24 K. J. Stevenson, *J. Am. Chem. Soc.*, 2011, **133**, 5621.
25 N. M. O'boyle, A. L. Tenderholt and K. M. Langner, *J. Comput. Chem.*, 2008, **29**, 839–845.
26 G. Zhurko and D. Zhurko, **https://www.chemcraftprog.com**, 2009.
27 K. Swaminathan, P. Narayanan, K. Sethusankar, V. Saravanan and A. K. Mohanakrishnan, *Acta Crystallogr., Sect. E: Struct. Rep. Online*, 2016, **72**, 1739–1743.
28 P. Geerlings and F. De Proft, *Phys. Chem. Chem. Phys.*, 2008, **10**, 3028–3042.
29 S. Sadiq, R. A. Khera, A. M. Tawfeek, M. A. Ibrahim, F. Abbas, S. Ali, A. Mahal, D. Meitao and M. Waqas, *J. Phys. Org. Chem.*, 2024, e4607.
30 A. Jezuita, K. Ejsmont and H. Szatylowicz, *Struct. Chem.*, 2021, **32**, 179–203.
31 S. A. Siddique, M. B. A. Siddique, R. Hussain, X. Liu, M. Y. Mehboob, Z. Irshad and M. Adnan, *Comput. Theor. Chem.*, 2020, **1191**, 113045.
32 A. Zahoor, N. Hadia, S. J. Akram, R. F. Mehmood, S. Sadiq, A. M. Shawky, N. S. Alatawi, A. Ahmed, J. Iqbal and R. A. Khera, *RSC Adv.*, 2023, **13**, 6530–6547.
33 C. Sandoval-Yañez and J. I. Martínez-Araya, *Chem. Phys. Lett.*, 2019, **715**, 354–359.
34 R. G. Parr and W. Yang, *J. Am. Chem. Soc.*, 1984, **106**, 4049–4050.
35 K. Fukui, *Science*, 1982, **218**, 747–754.
36 R. G. Parr, R. A. Donnelly, M. Levy and W. E. Palke, *J. Chem. Phys.*, 1978, **68**, 3801–3807.
37 R. Parthasarathi, J. Padmanabhan, M. Elango, V. Subramanian and P. Chattaraj, *Chem. Phys. Lett.*, 2004, **394**, 225–230.
38 R. G. Parr and R. G. Pearson, *J. Am. Chem. Soc.*, 1983, **105**, 7512–7516.
39 P. K. Chattaraj and D. R. Roy, *Chem. Rev.*, 2007, **107**, PR46–PR74.
40 M. Y. Mehboob, M. U. Khan, R. Hussain, K. Ayub, A. Sattar, M. K. Ahmad, Z. Irshad and M. Adnan, *Spectrochim. Acta, Part A*, 2021, **244**, 118873.
41 J. Padmanabhan, R. Parthasarathi, V. Subramanian and P. Chattaraj, *J. Phys. Chem. A*, 2007, **111**, 1358–1361.
42 F. A. Aloufi, R. F. Halawani, B. Jamoussi, A. K. Hajri and N. Zahi, *ACS Omega*, 2023, **8**, 21425–21437.
43 A. U. Hassan, S. H. Sumrra, M. Zubair, G. Mustafa, S. Noreen and M. Imran, *Chem. Pap.*, 2023, **77**, 6183–6202.
44 M. M. A. Iqbal, M. Y. Mehboob, R. Hussain, M. Adnan and Z. J, *Comput. Theor. Chem.*, 2021, **1202**, 113335.
45 M. Khalid, I. Shafiq, M. Zhu, M. U. Khan, Z. Shafiq, J. Iqbal, M. M. Alam, A. A. C. Braga and M. J, *J. Saudi Chem. Soc.*, 2021, **25**, 101305.
46 Z. Shuai, W. Li, J. Ren, Y. Jiang and H. Geng, *J. Chem. Phys.*, 2020, **153**, 080902.
47 M. Majeed, M. Waqas, R. F. Mehmood, N. S. Alatawi, M. Essid and R. A. Khera, *J. Phys. Chem. Solids*, 2023, **181**, 111495.
48 S.-J. Lee, J. B. Park, Y. S. Kim, H.-S. Shin, A. Kotta and H.-K. Seo, *Synth. Met.*, 2023, **294**, 117302.
49 Q. Zhao, S. Wang, Y.-H. Kim, S. Mondal, Q. Miao, S. Li, D. Liu, M. Wang, Y. Zhai and J. Gao, *Green Energy Environ.*, 2023, **9**, 949–965.
50 H. Tang, Y. Bai, H. Zhao, X. Qin, Z. Hu, C. Zhou, F. Huang and Y. Cao, *Adv. Mater.*, 2024, **36**, 2212236.
51 M. Khalid, S. Naz, K. Mahmood, S. Hussain, A. A. C. Braga, R. Hussain, A. H. Ragab and S. R. Al-Mhyawi, *RSC Adv.*, 2022, **12**, 31192–31204.
52 Z. Guo, A. K. Jena, G. M. Kim and T. Miyasaka, *Energy Environ. Sci.*, 2022, **15**, 3171–3222.
53 M. U. Saeed, J. Iqbal, R. F. Mehmood, S. J. Akram, Y. A. El-Badry, S. Noor and R. A. Khera, *Surf. Interfaces*, 2022, **30**, 101875.
54 M. C. Scharber, D. Mühlbacher, M. Koppe, P. Denk, C. Waldauf, A. J. Heeger and C. J. Brabec, *Adv. Mater.*, 2006, **18**, 789–794.
55 J. Fang, D. Deng, J. Zhang, Y. Zhang, K. Lu and Z. Wei, *Mater. Chem. Front.*, 2017, **1**, 1223–1228.
56 R. Hussain, M. Adnan, S. Nawab, M. U. Khan, M. Khalid, Z. Irshad, K. Ayub and J. Lim, *Synth. Met.*, 2022, **290**, 117159.
57 M. Khalid, I. Shafiq, M. Imran, R. Jawaria and A. A. C. Braga, *Synth. Met.*, 2024, **303**, 117548.
58 J. Contreras-García, E. R. Johnson, S. Keinan, R. Chaudret, J.-P. Piquemal, D. N. Beratan and W. Yang, *J. Chem. Theory Comput.*, 2011, **7**, 625–632.
59 E. R. Johnson, S. Keinan, P. Mori-Sánchez, J. Contreras-García, A. J. Cohen and W. Yang, *J. Am. Chem. Soc.*, 2010, **132**, 6498–6506.
60 I. Shafiq, R. Zahid, K. Mahmood, M. A. Asgha, T. Ahamad, S. Ahmed and S. C. Ojha, *J. Saudi Chem. Soc.*, 2023, **27**, 101767.